ACS SENSORS

pubs.acs.org/acssensors

Article

Living-Cell MicroRNA Imaging with Self-Assembling Fragments of Fluorescent Protein-Mimic RNA Aptamer

Yu Gu,* Li-Juan Huang, Wei Zhao,* Ting-Ting Zhang, Mei-Rong Cui, Xue-Jiao Yang, Xue-Li Zhao, Hong-Yuan Chen, and Jing-Juan Xu*

Cite This: *ACS Sens.* 2021, 6, 2339−2347

Read Online

ACCESS | Metrics & More | Article Recommendations | Supporting Information

ABSTRACT: As the cellular roles of RNA abundance continue to increase, there is an urgent need for the corresponding tools to elucidate native RNA functions and dynamics, especially those of short, low-abundance RNAs in live cells. Fluorescent RNA aptamers provide a useful strategy to create the RNA tag and biosensor devices. Corn, which binds with 3,5-difluoro-4-hydroxybenzylidene-imidazolinone-2-oxime (DFHO), is a good candidate for the RNA tag because of its enhanced photostability and red-shifted spectrum. Herein, we report for the first time the utilization of Corn as a split aptamer system, combined with RNA-initiated fluorescence complementation (RIFC), for monitoring RNA self-assembly and sensing microRNA. In this platform, the 28-nt Corn was divided into two nonfunctional halves (named probe I and probe II), and an additional target RNA recognition and stem part was introduced in each probe. The target RNA can trigger the self-assembly reconstitution of the Corn's G-quadruplex scaffold for DFHO binding and turn-on fluorescence. These probes can be transfected stably into mammalian cells and deliver the light-up fluorescent response to microRNA-21 (miR-21). Significantly, the probes have good photostability, with minimal fluorescence loss after continuous irradiation, and can be used for imaging of miR-21 in living mammalian cells. The proposed method is universal and could be applied to the sensing of other tumor-associated RNAs, including messenger RNA and noncoding RNA, as well as for monitoring RNA/RNA interactions. The Corn-based splitting aptamers show promising potential in the real-time visualization and mechanistic analysis of nucleic acids.

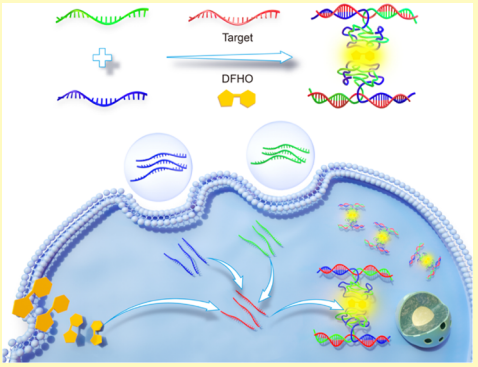

KEYWORDS: *microRNA imaging, RNA aptamers, G-quadruplexes, self-assembling, RNA-initiated fluorescence complementation*

MicroRNAs (miRNAs), the small noncoding RNA molecules, play crucial roles in RNA silencing and posttranscriptional regulation of gene expression.[1−3] The dysregulation of miRNAs often brings forth diseases including cancer,[4,5] nervous dysfunction,[6] and heart disease.[7] To monitor miRNA expression in physiological and pathological processes, generally the molecules have to be extracted and quantified using reverse transcriptase-polymerase chain reaction (RT-PCR).[8,9] However, RT-PCR is ex situ and suffers from the fast degradation of miRNAs. On the other hand, direct visualization of microRNAs in living cells using various optical methods provides dynamic information with better precision and quantification ability. Fluorescent in situ hybridization (FISH) assay has emerged as a prevailing method for imaging native DNA and RNA, which are inherently nonfluorescent.[10,11] FISH-based methods using programmable amplification allow the simultaneous imaging of multiple RNAs. Nonetheless, it often needs complicated target RNA engineering processes. In addition, FISH probes are only suitable for fixed cells rather than live-cell imaging.

With the abundance of newly discovered roles for miRNAs in biological systems, there is a growing need of the corresponding tools for in situ tracking them in living cells. In 2011, an RNA aptamer mimic of fluorescent protein that could bind and switch on the single-dye fluorescence of a noncytotoxic cell-permeable dye (3,5-difluoro-4-hydroxy-benzylidene midazolinone, DFHBI) was firstly reported.[12] This RNA−fluorophore complex, termed Spinach, allowed in situ visualization of RNAs in live cells, leading to new biological insights. Since then, the RNA aptamer−dye system has been improved with DFHBI analogues (such as DFHBI-1T-DFHBI with a 1,1,1-trifluoroethyl substituent and BI-bound Broccoli with higher affinity[13]) and with new versions of Spinach 2,[14] baby Spinach,[15] iSpinach,[16] and Broccoli,[17] which have attracted extensive attention in RNA imaging,[18−21] biological interaction,[22−24] and RNA-based fluorescent metabolite sensors.[25,26] The concept of split aptamers[27−30] or comple-

Received: March 2, 2021
Accepted: May 12, 2021
Published: May 24, 2021

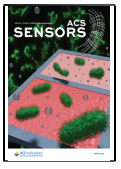

Table 1. Sequences Employed in This Work

name	sequences (5′-3′)
miR-21	rUrArGrCrUrUrArUrCrArGrArCrUrGrArUrGrUrUrGrA
M2	rUrArGrCrUrUrArUrCrArGrUrCrUrCrArUrGrUrUrGrA
Probe I	rUrCrArArCrArUrCrArArUrArUrGrCrGrArGrGrArArGrGrArGrGrUrCrUrGrA
Probe II	rGrGrArGrGrUrCrArCrUrGrCrArUrArArGrArUrArArGrCrUrA
AMO-miR-21	mU*mC*mA*mAmCmAmUmCmAmGmUmCmUmGmAmUmAmAmG*mC*mU*mA
Corn	rCrGrArArGrArArGrGrArGrGrUrCrUrGrArGrGrArGrGrUrCrArCrUrG
Broccoli	rGrArGrArCrGrGrUrCrGrGrGrUrCrCrArGrArUrArUrUrCrGrUrArUrCrUrGrUrCrGrArGrUrArGrArGrUrGrUrGrGrCrUrCrC

mentary nanoparticles[31] that are inactive until the halves are brought within close proximity or re-association by target can be useful for visualizing the actions of RNA and diverse functions. In 2017, Fan's group reported live-cell imaging of native RNA transcripts by engineering Broccoli and baby Spinach into two split fragments, which could bind to the target. After being genetically encoded in cells, the target mRNAs could bring the split parts into spatial proximity and result in turn-on fluorescence. The aptamer-initiated fluorescence complementation does not require prior modification of mRNA transcripts, which could be utilized for dynamic monitoring of mRNA.[32] Unfortunately, the spinach family or Broccoli-bound DFHBI exhibits rapid fluorescence decrease upon irradiation due to the light-induced isomerization of DFHBI to a nonfluorescent state, which is not conducive to long-term measurement.[21,33,34]

Recently, Song et al. described a 28-nt fluorescent protein-mimic turn-on RNA aptamer, Corn. It specifically binds with 3,5-difluoro-4-hydroxybenzylidene-imidazolinone-2-oxime (DFHO), and provides lower background, red-shifted fluorescence, and significantly enhanced photostability compared with DFHBI-based aptamers. This aptamer was used for time-resolved imaging of RNA polymerase III transcripts in HEK293T cells by expressing Corn driven by U6 promoter.[35] It was reported that the co-crystal structure of Corn−DFHO consisted of two molecules of Corn bound to a single DFHO molecule at its interprotomer interface as a 2:1 quasi-symmetric G-quadruplex homodimer and three non-base-paired adenosine residues from each protomer constituting the remainder of the binding site. It is worth noticing that six nucleotides in the interface of the Corn heterodimer adopt distinctly different conformations in the two protomers of identical sequence and break the symmetry. Thus, the RNA in the Corn−DFHO complex exhibits quasi-symmetry.[36] Because of its lack of stem−loop−stem structure and interprotomer base-paring, the modification and edition of Corn's structure is much difficult, but for such aptamers with excellent properties of low cytotoxicity, minimal background, compact size, and excellent photostability, expanding its further application to tagging and imaging of endogenous RNAs may offer new possibilities and soon become a general tool in RNA-based biological and medical analysis, as biologists have engaged for years with fluorescent proteins.

It was reported that two split nucleic acid probes containing parts of the G-quadruplex unit could form assembly of a full-length strand G-quadruplex structure after target sensing.[37,38] Given that Corn−DFHO binding is based on the G-quadruplex−DFHO−G-quadruplex sandwich structure, we assumed that two strands fused with parts of the Corn's sequence could by self-assembly refold the critical heterodimers for DFHO binding after specific recognition. In this work, we engineered an RNA-initiated fluorescence complementation (RIFC) system by splitting Corn into two fragments and each of them fused with the target recognition unit. When the target RNA was added, the two fragments could by self-assembly form a Corn-like G-quadruplex homodimer that could specifically bind to DFHO and switch on its fluorescence. The RNA probes are easy to synthesize, and the base sequence of the identified region can be changed according to practical demand, which is universal. This strategy can realize living-cell in situ fluorescence imaging of the native miRNA target without prior modification, and will open new avenues of using RNA aptamers in in vivo visualization analysis.

EXPERIMENTAL SECTION

Chemicals and Materials. DFHO from Lucerna Technologies, 2-ethanesulfonic acid (HEPES), thioflavin T, and thiazole orange were bought from Sigma-Aldrich Co. Ltd. Lipofectamine 3000 Transfection Teagent, Hoechst 33342, high-glucose Dulbecco's modified Eagle medium (DMEM), fetal bovine serum (FBS), and cell cytotoxicity assay kit (MTT) were purchased from Invitrogen. Diethyl pyrocarbonate (DEPC)-treated water was produced by Jiangsu Keygen Biotech. Corp. Ltd. and used in the preparation of all of the solutions. Precast-GL gel Native-PAGE (4−15%, 10 well) are prepared by Sangon Biotech (Shanghai, China). All of the RNAs reported in this approach were synthesized by Gen Script Co., Ltd. (Nanjing, China). All other reagents were of analytical grade. The sequences of the DNA and microRNA molecules are described in Table 1.

Spectroscopic Measurements of Aptamers. All RNAs were stored in diethyl pyrocarbonate (DEPC)-treated water at 10 μM concentrations in −20 °C refrigerator, respectively. All reagents were pre-warmed to 37 °C for 30 min before use. In all, 1 μM probe I and 1 μM probe II reacted with increasing concentrations of miR-21 for 2 h at 37 °C in a pH 7.4 buffer containing 20 μM DFHO, 100 mM KCl, 5 mM $MgCl_2$, and 40 mM HEPES before fluorescence measurement. Fluorescence spectra were recorded with excitation at 505 nm with a slit of size 5 nm for both the excitation and the emission.

Gel Electrophoresis Analysis. In the denaturing gradient gel electrophoresis assay, a Native-PAGE precast polyacrylamide gel with a 4−15% concentration gradient was chosen to improve the separation effect of RNA with slight molecular differences. In brief, 10 μL of the sample and 2 μL of 6× loading buffer were applied to individual lanes in a 4−15% polyacrylamide gel. Electrophoresis gels were run at 90 V for 40 min in running buffer (50 mM Tris, 50 mM HEPES, 2 mM ethylenediaminetetraacetic acid (EDTA), pH 7.9) in an ice−water mixture and then scanned using the gel image analysis system.

Cell Culture and MTT Assay. HeLa cells were cultured in high-glucose Dulbecco's modified Eagle's medium (DMEM) containing 10% fetal bovine serum and 1% penicillin/streptomycin at 37 °C in a humidified 5% CO_2 incubator. 1×10^4 cells were seeded into 96-well plates for 12 h. Then, probe I (200 ng/well) and probe II (200 ng/well) were transformed into the cells using Lipofectamine 3000 according to the manufacturer's instructions. Six hours later, the cells were washed with phosphate-buffered saline (PBS) and incubated in fresh DMEM for an additional 18 h. Then, 100 μL of MTT solution

https://doi.org/10.1021/acssensors.1c00453
ACS Sens. 2021, 6, 2339−2347

Scheme 1. Principle of Splitting Aptamer-Mediated RNA Recognition

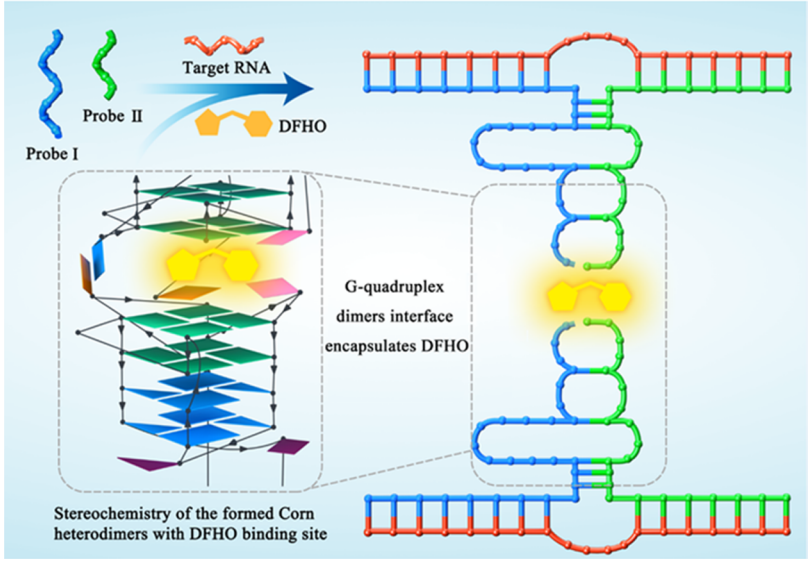

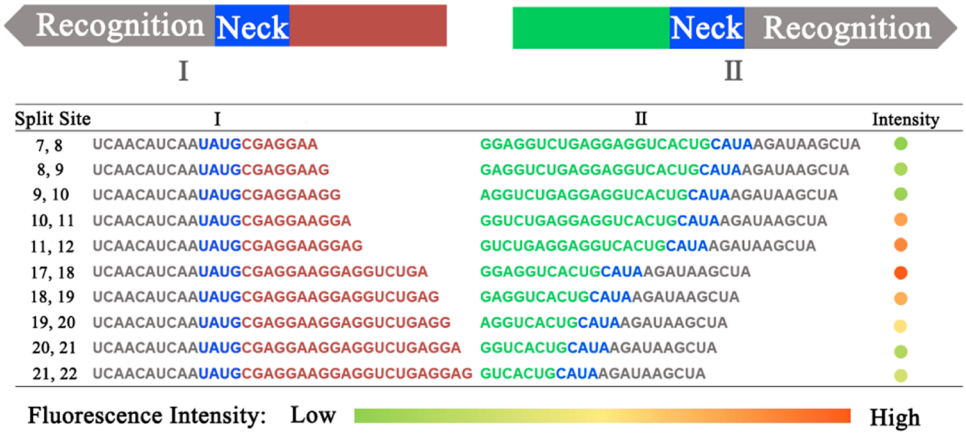

Figure 1. Fluorescence enhancement of split I and split II at different split sites incubated with the target RNA in HEPES buffer (40 mM, pH 7.4) containing 20 μM DFHO, 100 mM KCl, and 5 mM $MgCl_2$.

(0.5 mg/mL, PBS) was added to each well and stood for 4 h at 37 °C after washing three times with PBS. Then, the solution was discarded and 100 μL of dimethyl sulfoxide (DMSO) added to each well. The absorption intensity at 540 nm of each well was recorded after shaking for 5 min.

Live-Cell Imaging. HeLa cells were digested and incubated in confocal cell dishes (diameter: 10 mm) overnight and transfected with probe I and II for 6 h. Then, the cells were incubated with 20 μM DFHO for 30 min, Hoechst 33342 (5 μg/mL) for 15 min, and washed with PBS three times before confocal laser scanning microscopy imaging.

Flow Cytometry Analysis. HeLa cells were seeded into six-well plates (1×10^5 per well) for 24 h at 37 °C. Then, the cells were divided into three groups: group I was cultured with pure 1× opti-MEM MEM; group II was cultured with 1× opti-MEM for 6 h, then washed with PBS and incubated with DFHO; group III was transfected with probe I and II for 6 h, then rinsed with PBS three times, and incubated with DFHO in the same way as group II. After this, the cells were digested, concentrated (1000 rpm, 5 min), and washed with PBS three times. Finally, the cells were incubated with an apoptosis analysis reagent (Annexin V-FITC and PI) according to the manufacturer's instructions and then analyzed with flow cytometry.

RT-PCR Analysis. Total RNA samples were extracted from the cells using the Trizol reagent. Then, the samples were reversely transcribed into cDNAs using the SuperScript First-Strand Synthesis System (Invitrogen). The expression of miR-21 was determined using the TaqMan miRNA-assay (Sangon Biotech (Shanghai) Co., Ltd., China) and normalized by its relative expression to U6-snRNA; the sequence used in this analysis is shown in Table S1.

Statistical Analysis. All data were shown as mean ± standard deviations (SD). Data were plotted using originPro 2016 (OriginLab). Statistical analysis between the groups was performed by *t*-test. A *p*-value of <0.05 was considered statistically significant.

RESULTS AND DISCUSSION

Principle. Scheme 1 illustrates the working principle of the as-designed RIFC system, including target recognition, target-induced formation of the G-quadruplex homodimer, DFHO binding, and fluorescence enhancement of the system. The system consists of a target miRNA, two RNA probes, and the DFHO molecule. Both probe I and II contain a recognition block of target RNA and parts of Corn's unit. The two fragments I and II stay in the off state along with DFHO in the absence of the target (T). Once the T exists, fragments I and II are bought into proximity via complementary base pairing with T to generate the homodimer G-quadruplexes of Corn, sandwich structure of DFHO, and then turn-on fluorescence. We expected to build a novel RIFC system with superior

https://doi.org/10.1021/acssensors.1c00453
ACS Sens. 2021, 6, 2339−2347

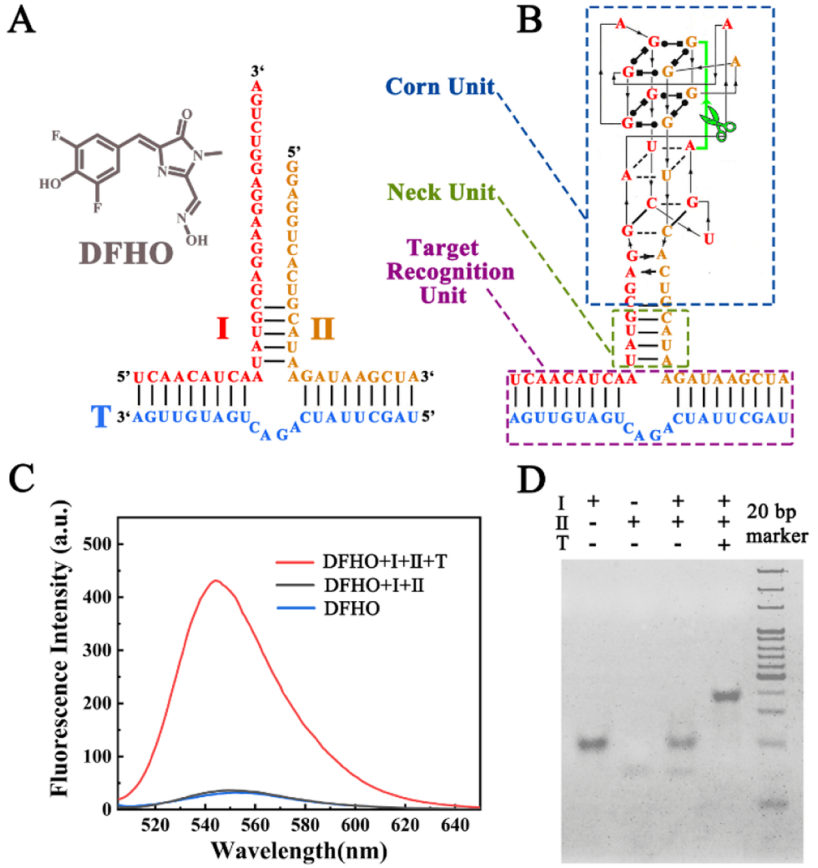

Figure 2. (A) Chemical structure of DFHO, sequence of I, II, and Target (T). (B) Secondary structure after I, II binding with T. (C) Fluorescence emission spectra of I, II (1 μM) in HEPES buffer (40 mM, pH 7.4) containing 20 μM DFHO, 100 mM KCl, and 5 mM $MgCl_2$ in the presence or absence of Target miR-21 (1 μM). (D) Native-PAGE results for the reaction of probe I and II with or without T; the "+" denotes the addition of these strands.

performance based on the advantages of good photostability and enhancement of the red-shifted fluorescence of our probes.

Split-Site Optimization. After comparing the free energies of the RNA aptamer secondary structures, we found that Corn has the most unstable structure with a free energy of −2.3 kcal/mol, which probably resulted from its lack of stem−loop−stem structure and interprotomer base pairing, while the values are −27.00, −33.80, and −11.60 kcal/mol for Spinach, Spinach 2, and Broccoli, respectively (Figure S1). The motif of Corn for RNA-induced small-molecule fluorescence was fully optimized. Truncation and mutations would affect its secondary structures. Therefore, two conditions must be met for the RIFC method to work successfully. First, each split fragment should have a specific target RNA recognition segment and abrogate its affinity toward the cognate fluorogen DFHO without the target RNA. Second, the Corn structure should be able to be reformed by hybridizing two split fragments with an RNA target to produce DFHO binders and induce fluorescence enhancement. We first split Corn into different G-quadruplex-related positions (from the 5′-end; the sequence of Corn is shown in Table 1), then extended the two split fragments each with a four-base-pair neck and 10-base RNA arms that were complementary to the target RNA (Figures 1 and S2). MicroRNA-21 (miR-21) was chosen as the target RNA because of its biological roles.[39] It turns out that probe I and II split between the 17th and 18th bases have the maximum fluorescence enhancement after incubation with DFHO and miR-21. The farther the split site from the 17th base, the smaller the fluorescence enhancement of DFHO. It also indicates that the 17th- and 18th-position bases are of great importance for the formation of the Corn's G-quadruplex structure. Hence, we chose to split Corn after the 17th nucleotide (from the 5′-end) into two fragments.

Validation of the RIFC Program. Figure 2A shows the sequence of the two probes and target RNA. MiR-21 can form a hybrid with our probes as it has 10 complementary base sequences with both I and II, respectively. According to the predicted two-dimensional (2D) structure of Corn (described in Figure 2B), the splitting aptamer-mediated RNA recognition system can be divided into three units: target recognition unit, neck unit, and "Corn" unit. The two toeholds after I, II binding with miR-21 could form the G-quadruplex structure, and two-G-quadruplex homodimer could encapsulate one molecule of DFHO at its interprotomer interface, thus inducing the fluorescence enhancement. To ensure proper operation of the entire program, the fluorescence spectrum and PAGE analysis are validated separately. As shown in Figure 2C, both DFHO and DFHO incubated with probe I and II have low, but measurable background fluorescence. When probe I and II were incubated with T in DFHO, the system exhibited considerable fluorescence enhancement with a maximum emission wavelength of 545 nm when excited at 505 nm. Polyacryamide gel electrophoresis (PAGE) analysis was done to further characterize the feasibility of this approach. As described in Figure 2D, two bands were observed for probe I and II, respectively. On mixing probe I with II for 2 h, no

https://doi.org/10.1021/acssensors.1c00453
ACS Sens. 2021, 6, 2339−2347

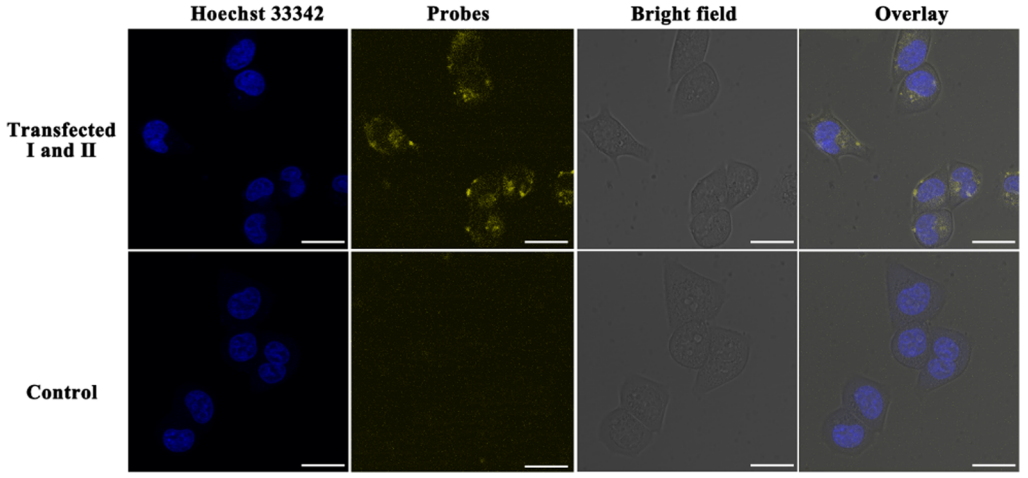

Figure 3. Live-cell confocal images of transcribed probe I and II with DFHO-targeted miR-21 in HeLa cells. Control cells are incubated only with DFHO. Scale bars = 25 μm.

additional bands appeared. However, on incubating miR-21 with probe I and II, a new band with a higher molecular weight of ~80 bp appeared, indicating the hybridization between I, II and the target RNA. No hybridization occurred when the target RNA was incubated with either probe I or probe II (Figure S3). It is probably because each of probe I and probe II has only 10 complementary bases with T, which is not stable for hybridization. In addition, as shown in Figure S4, there was a 79% loss of fluorescence intensity when the two-bases mismatch target (M2) was incubated with DFHO, I, and II. The above results indicate the good selectivity of these probes.

To further confirm the relationship between miR-21 and fluorescence enhancement, we incubated different concentrations of miR-21 with DFHO, I, and II (1 μM), and monitored the maximum emission peak. The results are described in Figure S5; a gradual fluorescence enhancement could be observed as the concentration of miR-21 increased. Furthermore, a good linear relationship was observed between the fluorescence intensity of the reaction products and the miR-21 concentration ranging from 0 to 1 μM. These experimental results indicated the feasibility of the system and that the proposed probe I and II system has good selectivity and linearity toward T. Subsequently, experiments were performed to confirm the structure of the products. Since the three-dimensional (3D) G-quadruplex structure of Corn is highly dependent on potassium in the buffer solution, other monovalent ions fail to promote G-quadruplex folding.[35] We tested whether the reaction of probe I and II incubated with T and DFHO yielded K^+-dependent aptamer-induced fluorescence. As expected (Figure S6), the enhancement of DFHO in Na^+-rich HEPES buffer was barely observed, whereas in HEPES buffer containing K^+, the fluorescence of DFHO showed significant enhancement. In addition, the enhancement obviously increased with the concentration of K^+ increasing from 0 to 100 mM in HEPES buffer. The fluorescence intensity was slightly lower when the K^+ concentration reached 200 mM, probably due to the fact that the folding efficiency of RNA can also be affected in a higher-ionic-strength environment. Our design of the RIFC method showed strong K^+ concentration dependence, suggesting that the G-quadruplex structure may be formed after the incubation of T with probe I and II. Furthermore, it was reported that small molecules such as thioflavin T or thiazole orange would emit fluorescence only when they bonded to the G-quadruplex structure.[35,36] Therefore, these two molecules were chosen to testify the overall structure of our re-synthesized Corn. As seen from Figures S7 and S8, the fluorescence intensities of thioflavin T and thiazole orange showed great enhancement when incubated with I, II, and T in HEPES buffer, confirming the formation of the G-quadruplex structure. Remarkably, the photostability of this complex was unique to DFHO. Although thioflavin T or thiazole orange could also produce Corn binders resulting in aptamer−fluorophore complexes, they are not photostable, which is the reason why we chose DFHO over other G-quadruplex-specific fluorescent dyes. The circular dichroism (CD) spectrum was also studied for the G-quadruplex characterization. As seen from Figure S9, the positive band at 270 nm and the negative band at 240 nm belong to the antiparallel and parallel quadruplexes, respectively. The small positive peak at 220 nm was the characteristic peak for both quadruplex types.[40] In addition, the CD spectrum of Corn alone and our probes after incubating with the target RNA matched well. All of the above experiments provide rich information on the structural configuration of Corn, like the G-quadruplex homodimer structure, after target recognition of our probes.

Cytotoxicity Test and Cellular Interference. The potential toxicity of RNA probes is a very crucial issue in biological studies. The MTT, being an important parameter to evaluate the potential toxicity of bioprobes, was measured after transfection of the probes. As described in Figure S10, no significant difference in the cell viability among HeLa cells treated with PBS, DFHO, probes, and the probes in DFHO-contained buffer was observed, which revealed that the proposed RNA probes showed excellent biocompatibility and low cytotoxicity in practical applications. Next, we examined whether the probes performed well in a complex biomatrix with the cellular environment. As described in Figure S11, compared with the HEPES buffer, the fluorescence intensity was decreased by 12% for the same concentration of miR-21 as used for incubation with our probes in the cell lysate, suggesting that the cell environment does affect the re-association efficiency (no significant differences) and it is probably caused by the relatively lower concentration of K^+ in cell. But this deviation is acceptable in cell imaging, and the RIFC method could be applicable in live-cell imaging.

https://doi.org/10.1021/acssensors.1c00453
ACS Sens. 2021, 6, 2339−2347

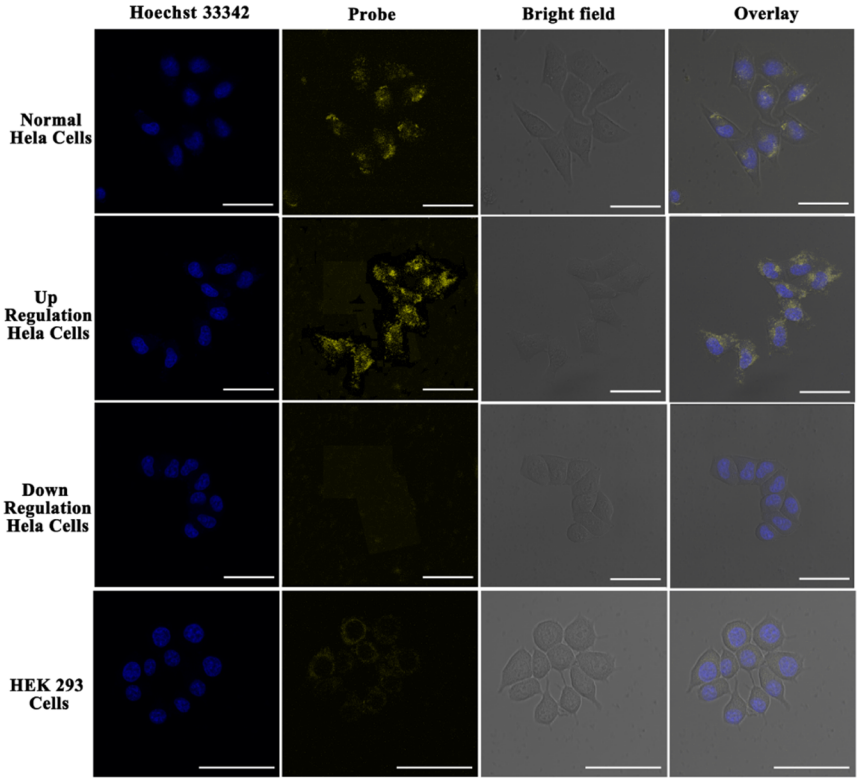

Figure 4. Confocal images of different regulations of HeLa cells and HEK293 cells transfected with probe I and II with DFHO. Scale bars = 50 μm.

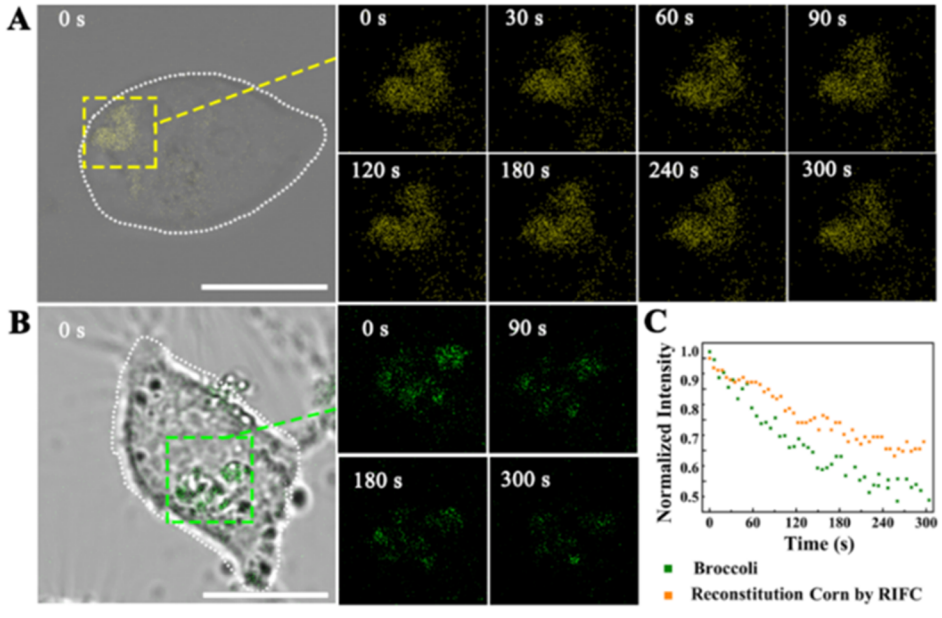

Figure 5. Time-resolved confocal images of cells transfected (A) with I and II with DFHO, (B) Broccoli by continuous irradiation and photography; scale bar: 25 μm. (C) Photostability of the two probes targeted with miR-21 in the presence of DFHO and Broccoli, separately.

Cell Imaging Studies of RIFC Probes. To testify whether the proposed probes could function well in detecting target RNA in living cells, cell imaging studies were performed with human epithelial carcinoma cancer (HeLa) cells that overexpressed miR-21.[41] HeLa cells were cotransfected with probe I and II, and then analyzed by confocal microscopy after incubating them with DFHO for 30 min. As illustrated in Figure 3, after transfection of probe I and II in the presence of DFHO, a strong diffuse yellow fluorescence signal was observed most prominently in the cytoplasma of HeLa cells under confocal microscopy, whereas the control cells incubated only with DFHO exhibited negligible fluorescence signals. Flow cytometric analysis further demonstrated the fluorescent difference of HeLa cells between the control group and the group cotransfected with probe I and II (Figure S12). The outcomes revealed that our probes exhibited good selectivity for miR-21 in cancer cells.[42−44]

https://doi.org/10.1021/acssensors.1c00453
ACS Sens. 2021, 6, 2339−2347

The levels of tumor-related microRNAs in cancer cells are related to the stages of tumor progression.[45,46] Further, we evaluated the effectiveness and robustness of the probes in the conditions with different miR-21 expression profiles. The anti-miRNA antisense inhibitor oligo deoxyribonucleotides (AMOs) were used to knock down miR-21 expression, while transfection of miR-21 was used to upregulate its level in HeLa cells. Untreated cells served as a control. It has been reported that miR-21 shows low expression in the HEK293 cell line. To testify the resolution of our probes for imaging miR-21 in other cells, HEK293 cells were cotransfected with probe I and II, and then analyzed by confocal microscopy after incubating with DFHO for 30 min. As seen from Figure 4, the fluorescence intensity was very weak in AMO-treated cells and higher in the upregulated miR-21 cells compared with normal cells, while HEK293 cells exhibited a slightly weaker fluorescence signal. TaqMan RT-PCR results (Figure S13) are consistent with the confocal results, further indicating that the fluorescence signal in the confocal images was positively correlated with the content of miR-21 within the HeLa cells. The results provide an ideal fluorescent reporter that enables dynamic mapping of miR-21 in living cells.

Photostability Investigation. The greatest advantage of Corn compared with other RNA aptamers is that it exhibits considerably improved photostability and enables live-cell imaging. We investigated the photostability of our probes in detecting target microRNA and commercially available DFHBI-based probes by continuous irradiation and photography every 1.293 s. As the principle of designing genetically encoded light-up DFHBI-based RNA aptamer sensors for imaging endogenous RNA is the reconstruction of these aptamers, Broccoli is the improved version of Spinach. Hence, we directly transfected Broccoli into HeLa cells for a more intuitive comparison. Figure 5 shows the time-dependent confocal images of HeLa cells by using probe I and II in the imaging of miR-21 in accordance with DFHO (Figure 5A and Video S1) and using Broccoli with DFHBI (Figure 5B). The fluorescence intensity of our probes incubated with DFHO-targeted miR-21 shows only an 8% decrease in the first 1 min, and a 25% decrease after 5 min of continuous irradiation. On the other hand, upon binding to DFHBI, Broccoli-tagged RNA exhibited marked photobleaching in living cells, amounting to more than 40% in 3 min and 51% loss in 5 min (Figure 5C). It is believed that mobility is related to the photodamage of several fluorophores. Broccoli revealed a binding site with limited hydrogen-bonding interactions with the DFHBI fluorophore, while the quasi-symmetry structure resulted from our RIFC recognition formed more hydrogen bonds with DFHO by comparison. DFHO fluorogen was locked into its planar conformation on top of the G-quadruplex region, thus reducing its mobility and preventing the formation of excited-state isomerization.[30] Our probe is demonstrated to exhibit good photostability, as well as Corn. Thus, these probes are proved to be capable for observation of gene expression levels in living cells.

CONCLUSIONS

In summary, the living-cell imaging of miRNAs provides a lot of information about the gene regulation of the corresponding mRNAs, tumor-related suppressors, and the oncogenic fragment. Here, we demonstrated a sensing approach using two programmable nucleic acid sequences split from the fluorescent protein-mimic turning-on RNA aptamer of Corn and fusing each of them with a target recognition sequence. With the addition of target RNA, the two fragments can be brought into proximity and form a Corn-like quasi-symmetric homodimer that could specifically bind with DFHO, thus markedly enhancing its fluorescence. Because of the specific target RNA recognition, the two probes can realize in situ cellular imaging of non-engineered, endogenous microRNA without prior modification. These RIFC methods exhibited the following advantages: (1) The split strategy required the target to hybridize with both split G4 parts simultaneously, thus rendering its good specificity and lower background; (2) As RNA probes can be simply synthesized and accurately changed, the method has universality as a similar monitoring program could be realized simply by redesigning the recognition unit of probe I and II according to the practical needs; (3) Compared to DFHBI aptamer-based recognition, the remarkable photostability of our approach makes it capable for imaging and qualitative analysis of nucleic acids, which is critical in clinical tumor screening. Nevertheless, it remains a challenge to screen a low abundance of the target as our strategy is still based on "one-to-one" triggered model. Since it is a generic concept, we believe that it is possible to sense low-copy-number intracellular RNAs by the introduction of the signal amplification strategy, and that is what we are going to do in the future. We believe the RIFC method can provide a powerful platform for and insights into miRNA function research in various biological applications.

ASSOCIATED CONTENT

Supporting Information

The Supporting Information is available free of charge at https://pubs.acs.org/doi/10.1021/acssensors.1c00453.

Sequences employed in PCR analysis, structure of RNA aptamer/fluorophore systems, selectivity and linearity, validation of G-quadruplexes structure, cytotoxicity test and cellular interference, flow cytometric analysis (PDF)

Representative miR-21 granule (yellow circle) with a total time of 300 s (Video S1) (AVI)

AUTHOR INFORMATION

Corresponding Authors

Yu Gu − *State Key Laboratory of Analytical Chemistry for Life Science and Collaborative Innovation Center of Chemistry for Life Sciences, School of Chemistry and Chemical Engineering, Nanjing University, Nanjing 210023, China; Institute for Materials Science and Engineering, School of Materials Sciences and Engineering, Suzhou University of Science and Technology, Suzhou 215011, China*; Email: guyujcb@163.com

Wei Zhao − *State Key Laboratory of Analytical Chemistry for Life Science, School of Chemistry and Chemical Engineering, Nanjing University, Nanjing 210023, China*; orcid.org/0000-0002-9526-2008; Phone: +86-25-89687294; Email: weizhao@nju.edu.cn

Jing-Juan Xu − *State Key Laboratory of Analytical Chemistry for Life Science, School of Chemistry and Chemical Engineering, Nanjing University, Nanjing 210023, China*; orcid.org/0000-0001-9579-9318; Phone: +86-25-89687294; Email: xujj@nju.edu.cn

https://doi.org/10.1021/acssensors.1c00453
ACS Sens. 2021, 6, 2339−2347

Authors

Li-Juan Huang − *State Key Laboratory of Analytical Chemistry for Life Science, School of Chemistry and Chemical Engineering, Nanjing University, Nanjing 210023, China*

Ting-Ting Zhang − *State Key Laboratory of Analytical Chemistry for Life Science, School of Chemistry and Chemical Engineering, Nanjing University, Nanjing 210023, China*

Mei-Rong Cui − *State Key Laboratory of Analytical Chemistry for Life Science, School of Chemistry and Chemical Engineering, Nanjing University, Nanjing 210023, China*

Xue-Jiao Yang − *State Key Laboratory of Analytical Chemistry for Life Science, School of Chemistry and Chemical Engineering, Nanjing University, Nanjing 210023, China*

Xue-Li Zhao − *College of Chemistry and Molecular Engineering, Zheng-Zhou University, Zhengzhou 450001, China*

Hong-Yuan Chen − *State Key Laboratory of Analytical Chemistry for Life Science, School of Chemistry and Chemical Engineering, Nanjing University, Nanjing 210023, China*

Complete contact information is available at: https://pubs.acs.org/10.1021/acssensors.1c00453

Author Contributions

Y.G. performed the experiments and wrote the manuscript. L.-J.H. collected some data. W.Z. administered the experiments and supervised the manuscript. T.-T.Z., M.-R.C., and X.-J.Y. analyzed the data. X.-L.Z. implemented the figures. H.-Y.C. and J.-J.X. validated the data and supervised the manuscript.

Notes

The authors declare no competing financial interest.

■ ACKNOWLEDGMENTS

This work was supported by the National Natural Science Foundation of China (21991080 and 21904092) and the Natural Science Foundation of Suzhou University of Science and Technology (XKZ2018007). This work was also supported by the Project Funded by State Key Laboratory of Analytical Chemistry for Life Science (SKLACLS 1909), Nanjing University.

■ REFERENCES

(1) Cheglakov, Z.; Cronin, T. M.; He, C.; Weizmann, Y. Live Cell MicroRNA Imaging Using Cascade Hybridization Reaction. *J. Am. Chem. Soc.* **2015**, *137*, 6116−6119.

(2) Zhang, P.; Cheng, F.; Zhou, R.; Cao, J.; Li, J.; Burda, C.; Min, Q.; Zhu, J. J. DNA-hybrid-gated multifunctional mesoporous silica nanocarriers for dual-targeted and microRNA-responsive controlled drug delivery. *Angew. Chem., Int. Ed.* **2014**, *53*, 2371−2375.

(3) Zhang, N.; Ye, S. J.; Wang, Z. X.; Li, R. H.; Wang, M. L. A Dual-Signal Twinkling Probe for Fluorescence-SERS Dual Spectrum Imaging and Detection of miRNA in Single Living Cell via Absolute Value Coupling of Reciprocal Signals. *ACS Sens.* **2019**, *4*, 924−930.

(4) Feng, Y. C.; Liu, X. Y.; Teng, L.; Ji, Q.; Wu, Y.; Li, J. M.; Gao, W.; Zhang, Y. Y.; La, T.; Tabatabaee, H.; Yan, X. G.; Jamaluddin, M. F. B.; Zhang, D.; Guo, S. T.; Scott, R. J.; Liu, T.; Thorne, R. F.; Zhang, X. D.; Jin, L. c-Myc inactivation of p53 through the pan-cancer lncRNA MILIP drives cancer pathogenesis. *Nat. Commun.* **2020**, *11*, No. 4980.

(5) Zhang, Y.; Dutta, A.; Abounader, R. The role of microRNAs in glioma initiation and progression. *Front. Biosci.* **2012**, *17*, 700−712.

(6) Kiltschewskij, D.; Cairns, M. J. Temporospatial guidance of activity-dependent gene expression by microRNA: mechanisms and functional implications for neural plasticity. *Nucleic Acids Res.* **2019**, *47*, 533−545.

(7) Chen, K. T.; Liao, Y. L. Identification of mRNA and microRNA profiles in right ventricular dysfunction induced type II cardiorenal syndrome. *Eur. Heart J.* **2020**, *41*, 3809.

(8) Calin, G. A.; Liu, C. G.; Sevignani, C.; Ferracin, M.; Felli, N.; Dumitru, C. D.; Shimizu, M.; Cimmino, A.; Zupo, S.; Dono, M.; Dell'Aquila, M. L.; Alder, H.; Rassenti, L.; Kipps, T. J.; Bullrich, F.; Negrini, M.; Croce, C. M. MicroRNA profiling reveals distinct signatures in B cell chronic lymphocytic leukemias. *Proc. Natl. Acad. Sci. U.S.A.* **2004**, *101*, 11755−11760.

(9) Chen, C. F.; Ridzon, D. A.; Broomer, A. J.; Zhou, Z. H.; Lee, D. H.; Nguyen, J. T.; Barbisin, M.; Xu, N. L.; Mahuvakar, V. R.; Andersen, M. R.; Lao, K. Q.; Livak, K. J.; Guegler, K. J. Real-time quantification of microRNAs by stem−loop RT−PCR. *Nucleic Acids Res.* **2005**, *33*, No. e179.

(10) He, J.; Mo, D.; Chen, J.; Luo, L. Combined whole-mount fluorescence in situ hybridization and antibody staining in zebrafish embryos and larvae. *Nat. Protoc.* **2020**, *15*, 3361−3379.

(11) Lu, J.; Tsourkas, A. Imaging individual microRNAs in single mammalian cells in situ. *Nucleic Acids Res.* **2009**, *37*, No. e100.

(12) Paige, J. S.; Wu, K. Y.; Jaffrey, S. R. RNA Mimics of Green Fluorescent Protein. *Science* **2011**, *333*, 642−646.

(13) Li, X.; Kim, H.; Litke, J. L.; Wu, J. H.; Jaffrey, S. R. Fluorophore-promoted RNA folding and photostability enable imaging of single Broccoli-tagged mRNAs in live mammalian cells. *Angew. Chem., Int. Ed.* **2020**, *59*, 4511−4518.

(14) Strack, R. L.; Disney, M. D.; Jaffrey, S. R. A super folding Spinach2 reveals the dynamic nature of trinucleotide repeat−containing RNA. *Nat. Methods* **2013**, *10*, 1219−1224.

(15) Warner, K. D.; Chen, M. C.; Song, W.; Strack, R. L.; Thorn, A.; Jaffrey, S. R.; Ferre-D'Amare, A. R. Structural basis for activity of highly efficient RNA mimics of green fluorescent protein. *Nat. Struct. Mol. Biol.* **2014**, *21*, 658−663.

(16) Autour, A.; Westhof, E.; Ryckelynck, M. iSpinach: a fluorogenic RNA aptamer optimized for in vitro applications. *Nucleic Acids Res.* **2016**, *44*, 2491−2500.

(17) Filonov, G. S.; Moon, J. D.; Svensen, N.; Jaffrey, S. R. Broccoli: Rapid Selection of an RNA Mimic of Green Fluorescent Protein by Fluorescence-Based Selection and Directed Evolution. *J. Am. Chem. Soc.* **2014**, *136*, 16299−16308.

(18) Aw, S. S.; Tang, M. X.; Teo, Y. N.; Cohen, S. M. A conformation-induced fluorescence method for microRNA detection. *Nucleic Acids Res.* **2016**, *44*, No. 92.

(19) Chen, X.; Zhang, D.; Su, N.; Bao, B.; Xie, X.; Zuo, F.; Yang, L.; Wang, H.; Jiang, L.; Lin, Q.; Fang, M.; Li, N.; Hua, X.; Chen, Z.; Bao, C.; Xu, J.; Du, W.; Zhang, L.; Zhao, Y.; Zhu, L.; Loscalzo, J.; Yang, Y. Visualizing RNA dynamics in live cells with bright and stable fluorescent RNAs. *Nat. Biotechnol.* **2019**, *37*, 1287−1293.

(20) Jepsen, M. D. E.; Sparvath, S. M.; Nielsen, T. B.; Langvad, A. H.; Grossi, G.; Gothelf, K. V.; Andersen, E. S. Development of a genetically encodable FRET system using fluorescent RNA aptamers. *Nat. Commun.* **2018**, *9*, No. 18.

(21) Swetha, P.; Fan, Z.; Wang, F.; Jiang, J. H. Genetically encoded light-up RNA aptamers and their applications for imaging and biosensing. *J. Mater. Chem. B* **2020**, *8*, 3382−3392.

(22) Alam, K. K.; Tawiah, K. D.; Lichte, M. F.; Porciani, D.; Burke, D. H. A fluorescent split aptamer for visualizing RNA-RNA assembly in vivo. *ACS Synth. Biol.* **2017**, *6*, 1710−1721.

(23) Rogers, T. A.; Andrews, G. E.; Jaeger, L.; Grabow, W. W. Fluorescent monitoring of RNA assembly and processing using the split-spinach aptamer. *ACS Synth. Biol.* **2015**, *4*, 162−166.

(24) Roszyk, L.; Kollenda, S.; Hennig, S. Using a specific RNA-protein interaction to quench the fluorescent RNA spinach. *ACS Chem. Biol.* **2017**, *12*, 2958−2964.

(25) Paige, J. S.; Nguyen-Duc, T.; Song, W.; Jaffrey, S. R. Fluorescence imaging of cellular metabolites with RNA. *Science* **2012**, *335*, 1194.

(26) You, M.; Litke, J. L.; Jaffrey, S. R. Imaging metabolite dynamics in living cells using a Spinach-based riboswitch. *Proc. Natl. Acad. Sci. U.S.A.* **2015**, *112*, E2756−E2765.

(27) Sajja, S.; Chandler, M.; Striplin, C. D.; Afonin, K. A. Activation of Split RNA Aptamers: Experiments Demonstrating the Enzymatic Synthesis of Short RNAs and Their Assembly As Observed by Fluorescent Response. *J. Chem. Educ.* **2018**, *95*, 1861−1866.
(28) Panigaj, M.; Johnson, M. B.; Ke, W.; McMillan, J.; Goncharova, E. A.; Chandler, M.; Afonin, K. A. Aptamers as Modular Components of Therapeutic Nucleic Acid Nanotechnology. *ACS Nano* **2019**, *13*, 12301−12321.
(29) Kolpashchikov, D. M. Binary malachite green aptamer for fluorescent detection of nucleic acids. *J. Am. Chem. Soc.* **2005**, *127*, 12442−12443.
(30) Chandler, M.; Lyalina, T.; Halman, J.; Rackley, L.; Lee, L.; Dang, D.; Ke, W.; Sajja, S.; Woods, S.; Acharya, S.; Baumgarten, E.; Christopher, J.; Elshalia, E.; Hrebien, G.; Kublank, K.; Saleh, S.; Stallings, B.; Tafere, M.; Striplin, C.; Afonin, K. A. Broccoli Fluorets: Split Aptamers as a User-Friendly Fluorescent Toolkit for Dynamic RNA Nanotechnology. *Molecules* **2018**, *23*, No. 3178.
(31) Halman, J. R.; Satterwhite, E.; Roark, B.; Chandler, M.; Viard, M.; Ivanina, A.; Bindewald, E.; Kasprzak, W. K.; Panigaj, M.; Bui, M. N.; Lu, J. S.; Miller, J.; Khisamutdinov, E. F.; Shapiro, B. A.; Dobrovolskaia, M. A.; Afonin, K. A. Functionally-interdependent shape-switching nanoparticles with controllable properties. *Nucleic Acids Res.* **2017**, *45*, 2210−2220.
(32) Wang, Z.; Luo, Y.; Xie, X.; Hu, X.; Song, H.; Zhao, Y.; Shi, J.; Wang, L.; Glinsky, G.; Chen, N.; Lal, R.; Fan, C. H. In situ spatial complementation of aptamer-mediated recognition enables live-cell imaging of native RNA transcripts in real time. *Angew. Chem., Int. Ed.* **2018**, *57*, 972−976.
(33) Engelhart, A. E. RNA imaging: A tale of two G-quadruplexes. *Nat. Chem. Biol.* **2017**, *13*, 1140−1141.
(34) Su, Y.; Hammond, M. C. RNA-based fluorescent biosensors for live cell imaging of small molecules and RNAs. *Curr. Opin. Biotechnol.* **2020**, *63*, 157−166.
(35) Song, W.; Filonov, G. S.; Kim, H.; Hirsch, M.; Li, X.; Moon, J. D.; Jaffrey, S. R. Imaging RNA polymerase III transcription using a photostable RNA-fluorophore complex. *Nat. Chem. Biol.* **2017**, *13*, 1187−1194.
(36) Warner, K. D.; Sjekloca, L.; Song, W.; Filonov, G. S.; Jaffrey, S. R.; Ferre-D'Amare, A. R. A homodimer interface without base pairs in an RNA mimic of red fluorescent protein. *Nat. Chem. Biol.* **2017**, *13*, 1195−1201.
(37) Shimron, S.; Wang, F.; Orbach, R.; Willner, I. Amplified detection of DNA through the enzyme-free autonomous assembly of hemin/G-quadruplex DNAzyme nanowires. *Anal. Chem.* **2012**, *84*, 1042−1048.
(38) Gu, Y.; Song, J.; Li, M. X.; Zhang, T. T.; Zhao, W.; Xu, J. J.; Liu, M. L.; Chen, H. Y. Ultrasensitive MicroRNA assay via surface plasmon resonance responses of Au@Ag nanorods etching. *Anal. Chem.* **2017**, *89*, 10585−10591.
(39) Wang, L.; Liu, P. F.; Liu, Z. J.; Zhao, K. R.; Ye, S. Y.; Liang, G. X.; Zhu, J. J. Simple Tripedal DNA Walker prepared by target-triggered catalytic hairpin assembly for ultrasensitive electrochemiluminescence detection of microRNA. *ACS Sens.* **2020**, *5*, 3584−3590.
(40) Kypr, J.; Kejnovska, I.; Renciuk, D.; Vorlickova, M. Circular dichroism and conformational polymorphism of DNA. *Nucleic Acids Res.* **2009**, *37*, 1713−1725.
(41) Peng, H.; Newbigging, A. M.; Reid, M. S.; Uppal, J. S.; Xu, J.; Zhang, H.; Le, X. C. Signal Amplification in Living Cells: A review of microRNA detection and imaging. *Anal. Chem.* **2020**, *92*, 292−308.
(42) Calin, G. A.; Croce, C. M. MicroRNA signatures in human cancers. *Nat. Rev. Cancer* **2006**, *6*, 857−866.
(43) Lu, J.; Getz, G.; Miska, E. A.; Alvarez-Saavedra, E.; Lamb, J.; Peck, D.; Sweet-Cordero, A.; Ebet, B. L.; Mak, R. H.; Ferrando, A. A.; Downing, J. R.; Jacks, T.; Horvitz, H. R.; Golub, T. R. MicroRNA expression profiles classify human cancers. *Nature* **2005**, *435*, 834−838.
(44) Volinia, S.; Calin, G. A.; Liu, C. G.; Ambs, S.; Cimmino, A.; Petrocca, F.; Visone, R.; Iorio, M.; Roldo, C.; Ferracin, M.; Prueitt, R. L.; Yanaihara, N.; Lanza, G.; Scarpa, A.; Vecchione, A.; Negrini, M.; Harris, C. C.; Croce, C. M. A microRNA expression signature of human solid tumors defines cancer gene targets. *Proc. Natl. Acad. Sci. U.S.A.* **2006**, *103*, 2257−2261.
(45) Haigl, B.; Vanas, V.; Setinek, U.; Hegedus, B.; Gsur, A.; Sutterluety-Fall, H. Expression of microRNA-21 in non- small cell lung cancer tissue increases with disease progression and is likely caused by growth conditional changes during malignant transformation. *Int. J. Oncol.* **2014**, *44*, 1325−1334.
(46) Negoi, I.; Hostiuc, S.; Sartelli, M.; Negoi, R. I.; Beuran, M. MicroRNA-21 as a prognostic biomarker in patients with pancreatic cancer − A systematic review and meta-analysis. *Am. J. Surg.* **2017**, *214*, 515−524.

https://doi.org/10.1021/acssensors.1c00453
ACS Sens. 2021, 6, 2339−2347